PAPER

Crab-inspired compliant leg design method for adaptive locomotion of a multi-legged robot

View the article online for updates and enhancements.

You may also like

Bioinspiration & Biomimetics

Crab-inspired compliant leg design method for adaptive locomotion of a multi-legged robot

Jun Zhang*[iD], Qi Liu[iD], Jingsong Zhou[iD] and Aiguo Song[iD]

The State Key Laboratory of Bioelectronics, School of Instrument Science and Engineering, Southeast University, 210096, People's Republic of China
* Author to whom any correspondence should be addressed.

E-mail: j.zhang@seu.edu.cn

Abstract

Chinese mitten crab has unique limb structures composed of a hard exoskeleton and flexible muscles. They enable the crab to locomote adaptively and safely on various terrains. In this work, we investigated the limb structures, motion principle, and gaits of the crab using a high-speed camera and a press machine. Then, a novel compliant robot leg design method is proposed, inspired by the crab limb. The leg comprises six hard scleromeres and a flexible thin-wall spring steel sheet (FSSS) mimicking the exoskeleton and muscle. The scleromeres connected one by one with rotational joints are designed with slots. The front end of the FSSS is fixed on the scleromere close to the ground. The rear end crosses the slots and is mounted at the shaft of a linear actuator installed at the rear scleromere. The leg bends and stretches when the actuator pushes and pulls the FSSS, respectively. The kinematic modeling, rigid-flexible coupling dynamic simulations, and leg prototype tests are conducted, which verify the leg design approach. Thirdly, we put forward a multi-legged robot with eight compliant legs and design its gait using the gaits of the crab. Finally, the robot's performance is evaluated, including the capabilities of walking on different terrains at adjustable speeds and body heights, traversing low channels, walking on slopes, and carrying loads. The results prove that the single-motor-actuated compliant legs and their dynamic coupling with the rigid robot body frame can enable them to have the ground clearance ability and realize the adaptive walking of the robot. The leg design methodology can be used to design multi-legged robots with the merits of compact, light, low mechanical complexity, high safety, and easy to control, for many applications, such as environmental monitoring, search and rescue.

1. Introduction

Animals and insects use the legged locomotion pattern in nature to traverse uneven terrain for millions of years. Inspired by these creatures, researchers had designed a variety of legged robots [1] which possessed better mobility and adaptability to terrain irregularities than wheeled robots [2]. In the last decades, a significant number of multi-legged robots [3–6] were developed, inspired by dogs, cockroaches, spiders, and crabs for operating in the unstructured environment. For example, the BigDog built by Boston Dynamics could travel in outdoor steep and rough terrains [7]. The MIT Cheetah quadruped robot was able to bounce and jump over 40 cm high obstacles [8]. The cockroach-inspired hexapod robot

RHex was capable of reliably climbing various sizes of stairs [9]. The hexapod inspired by cockroaches had the ability to climb a step as high as 2.3 times its leg length [10]. Furthermore, eight-legged robots with higher stability than quadrupeds and hexapods were developed. Robug IV was an eight-legged robot with efficient walking gaits [2]. Each leg of Robug IV was composed of two rigid links and four joints. Lobster was an American lobster-inspired multi-legged robot for remote-sensing operations underwater [11]. Spider-bot was an eight-legged robot realized by NASA to work on the rough terrain of the outer planet [12]. Crabster-CR200 was a crab-inspired hexapod robot for underwater search and rescue [13]. The crablike robot with multiple redundant legs had a self-adaptive gait and slope climbing ability [14]. The

tapered and curved feet were designed for the legs of a crablike robot to walk on sandy and rocky terrain [15].

In order to locomote agilely on the uneven ground, dedicated gaits design, motion trajectory planning, precise ground condition sensing, and coordinated legs control are usually required for legged robots with rigid legs and joints. The rigid legs have the advantages of high motion precision and payload capability. However, high control precision is usually needed during touching the ground for these legs which lack compliance. Therefore, many methods are adopted by legged robots to realize adaptive locomotion.

One method is designing intelligent control algorithms with detections of the body posture, joint torque, ground contact force, etc, during locomotion. Kimura *et al* adopted the central pattern generator based control method for a quadruped robot to walk adaptively on unknown irregular terrain [16]. Buchli *et al* presented an adaptive frequency oscillators-based locomotion controller for a compliant quadruped robot to track its body properties [17]. Lee *et al* employed the reinforcement learning algorithm to the obstacles negotiation of a quadruped robot that can successfully climb over various obstacles [18]. Hwangbo *et al* transferred a neural network control policy trained in simulation to the quadruped robot ANYmal which demonstrated better velocity following ability and faster running speed [19]. Zhang *et al* proposed a contact force estimation method for the impedance control of the legged robot to obtain compliance in stable motion [20]. Goldschmidt *et al* introduced an adaptive neural control mechanism applied to a hexapod robot for obstacle negotiation in different walking gaits [21]. Luk *et al* used genetic algorithms to find optimal walking gaits for the eight-legged robot [2].

Another approach is using compliant and even soft mechanical structures and actuators in legged robot design. These elements make up compliant and soft joints with the biological characteristics of environment adaptability compared to stiff ones. As a result, the compliant robots have higher robustness, flexibility, and safety [22]. Liu *et al* proposed a switchable parallel elastic actuator-based robot with leg stiffness adjustment capability inspired by the compliant elements in animal motion [23]. Sproewitz *et al* presented a compliant quadruped robot with distal in-series elasticity that showed improved stability and maximum speed than the stiffer robot [24]. Hutter *et al* utilized the compliant series elastic actuators to design the compliant quadruped robot StarlETH realizing high energy efficiency and dynamic maneuvers [25]. Gor *et al* designed telescopic compliant legs for a quadruped robot which was more energy-efficient than rigid legged robots [26]. Hoffmann and Simanek presented a quadruped robot with four passively compliant knee joints

enabling it to move faster and more stable than those with actuated knee joints [27]. Kanner *et al* put forward the non-redundant design strategy for legged robots passively adapting to rough terrain [28]. Lakatos *et al* developed a quadruped robot with compliantly actuated legs for pronking, trotting, and dynamic walking [29]. Sun and Zhao studied a novel reconfigurable mechanism by embedding shape morphing into the joints of legged robots to achieve multiple trajectories [30]. Sharbafi *et al* employed passively compliant elements in legged robots design to cope with uncertainties instead of adjusting the controller because it may be influenced by the measurement delays and noise [31]. SMoLBot was an eight-legged robot with soft and rigid compliant backbones for gait studying of the locomotion of legged modular robots [32]. SILVER2 was a crab-inspired underwater hexapod robot equipping with SEAs in its tibia joints to traverse irregular terrains with a hopping gait [33]. The shoal crablike underwater robot also had the bounding gait which significantly improved the robot's average motion speed and energy efficiency compared with the bionic wave gait [34].

Soft materials are employed for the construction of more flexible legs of robots. These robots have higher safety and adaptability in crossing narrow spaces and cluttered environments. Kim *et al* reviewed the soft robots which have low mechanical and control complexities and can interact with unpredictable environments adaptively and flexibly [35]. Inspired by squid, starfish, and worms, Shepherd *et al* designed an elastomeric polymer-based soft quadruped robot capable of navigating different obstacles [36]. Fang *et al* studied a compliant flipper-leg for an amphibious robot to conquer complex environments [37]. Kaln *et al* developed a quadruped robot made of soft materials for legs, body, and circuit board, enabling the robot to overcome obstacles better than the rigid robots [38]. Zhou *et al* studied the control of the twisted artificial muscles for a bionic soft hexapod robot with the multi-motion ability [39].

Although the soft robots have the merits of large deformation capability and environment adaptability, they have a low load capacity. In the nature, animals and insects with musculoskeletal systems can move fast and agile on almost all ground terrains providing inspiration for legged robot design. In this paper, we present a multi-legged robot with compliant legs and investigate the adaptive locomotion of the robot based on experimental studies on the locomotion gaits of the *Chinese mitten crab*. The main contributions of this work are as follows: (1) A novel compliant robot leg design method is proposed, inspired by the rigid-flexible structure, protection function, and motion principle of the crab limb, which proves, in turn, the biological superiority of crab legs' structure and function from an engineering point of view; (2) the multi-legged robot with the compliant legs is

put forward, and its gait is designed by mimicking the locomotion pattern of crabs and taking advantage of the rigid-flexible dynamic coupling among the rigid body frame and compliant legs. The dynamic coupling among the compliant legs and rigid body frame enables the robot to have the ground clearance ability and walk adaptively on different terrains, travel channels, climb slopes, and even carry heavy loads for various applications. Simulations and experiments verify this new legged robot design method and its locomotion performance. The details are introduced in the rest of the paper.

2. Crab locomotion mechanism

The locomotion mechanism of the *Chinese mitten crab* was studied firstly before the multi-legged robot design. We investigated the structure and motion principle of the crab limb, which gives inspiration for the novel compliant leg design and the locomotion gait design of the robot.

2.1. Crab limb structure and motion principle
As shown in figure 1(a), the *Chinese mitten crab* has one pair of claws and four pairs of walking legs composed of the hard exoskeleton and flexible muscles. Each walking leg consists of six segments, i.e. basipodite, ischiopodite, meropodite, carpopodite, propodite, and dactylopodit. The hard exoskeleton of the legs comprising chitin [40] provides the crab with powerful protection from outer impacts and injury. The leg joints are driven to bend or stretch through the pull and contraction of the flexible different antagonistic muscles in the exoskeleton. Hence, the rigid-flexible skeletal muscle system of the legs has good strength and flexibility which enable crabs to interact with the ground naturally and safely.

Figure 1(b) illustrates the arrangement of essential muscles that realize the movement of the crab limb [41]. The bender and stretcher in the gaiter are similar to the antagonist muscles in the human body. The extension and contraction of the opener and closer muscles pull the joints to realize movements of different degrees of freedom.

The structure of the crab limbs provides new ideas for designing the rotational joint and actuation method of the compliant robot leg. A crab-limb-inspired novel joint mechanism for the legged robot is designed as illustrated in figure 1(c). The mechanism consists of two rigid scleromeres and a FSSS. The rigid scleromeres play the role of the exoskeleton in protecting the internal muscles. The FSSS housed in the rigid scleromeres mimics the principle of the antagonizing muscles of the crab limb. The FSSS has the advantage of providing not only the pushing force during leg bending but also the pulling force during leg stretching.

We also tested the load capability of the hard exoskeleton of carb limbs for designing and optimizing the scleromeres of the robot legs in section 3.1. In the experiments, 11 *Chinese mitten crabs* with a maximum width of 55.59 ± 1.86 mm of their carapaces and a weight of 289.42 ± 6.01 g were selected. Leg 2 of the crabs were used in the tests. The maximum width and thickness of the legs and their exoskeleton thickness were 10.35 ± 0.45 mm, 4.92 ± 0.19 mm, and 0.23 ± 0.03 mm, respectively. The scenario of the test with a press machine is depicted in figure 2(a). The leg was fixed to a fixture. Then, the scleromere meropodite was pressed by the machine. The recorded deformation of the scleromere and the pressure are shown in figure 2(b). The results indicate that the hard exoskeleton has high load capability and good protection function on the soft muscles. This characteristic inspired us to design the robot legs with a similar hard exoskeleton for protecting the inner flexible actuation mechanism.

2.2. Crab motion patterns and gaits
Crabs have unique motion patterns. They usually move fast with the lateral motion pattern while sometimes also can move with the forward movement pattern [42]. They change gaits at different mediums [14] to improve the walking efficiency and minimize the risk of injury in the event of a misstep [43]. In order to design a proper gait for the multi-legged robot, we studied the motion patterns of the 11 *Chinese mitten crabs* by experiments and statistical analysis. In the experiments, the crabs were put in a plastic box with its bottom covered by the carpet. The crabs could move freely in the box. A high-speed camera with a frame rate of 240 fps and resolution of 1920 × 1080 pixels was mounted over the box for recording the locomotion of the crabs. Each of the crabs was tested at least five times. A minimum of 3 walking videos with an even sideways gait, a straight path, and at least three gait cycles for each crab was selected for analysis. A total of 40 walking videos of the 11 crabs were selected for statistical analysis. The video was analyzed frame by frame to obtain the stepping patterns of the crabs. The foot tip was considered as contacting the ground when the lateral displacement ceases [43].

The results in figure 3(a) depict ten selected video sequences of the sideway locomotion process of one crab. Figure 3(b) shows the timing of the steps of the crab's eight legs from the video in (a). L1 to L4 are the leading legs. T1 to T4 are the trailing legs. The black bars represent the support phases, and the white bars represent the transfer phases. The stepping pattern is a typical zigzag gait [14]. In the first period, legs L2 and L4 on the leading side and T1 and T3 on the trailing side are in the transfer phase, while L1, L3, T2, and T4 are in the support phases. Then the two groups switch their phase states alternately for adaptive walking.

The statistical analysis results of the gait models used by the crabs are shown in figure 3(c). The metachronal model (M) means the adjacent legs step one by one, such as L1–L2–L3–L4. The alternating tetrapod model (A) is based on alternating of the
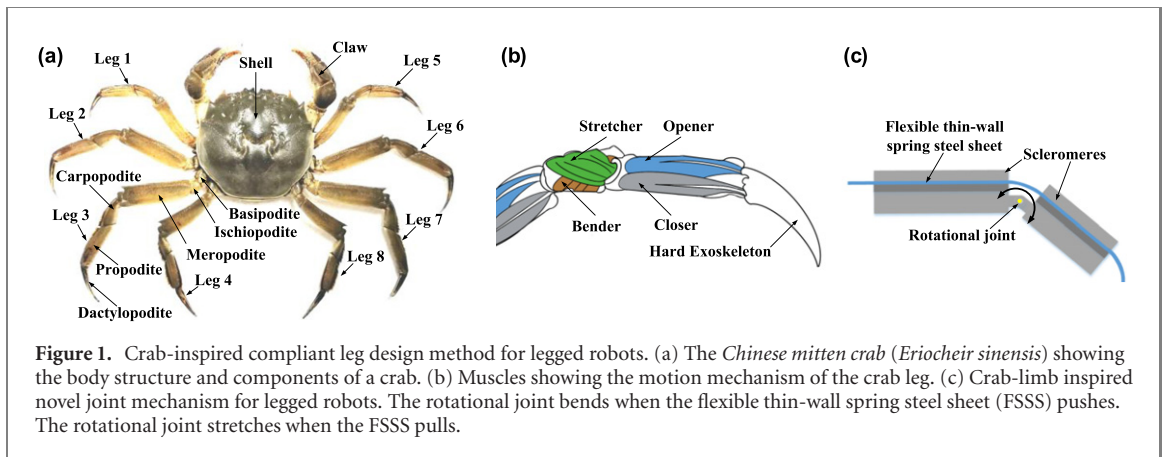
Figure 1. Crab-inspired compliant leg design method for legged robots. (a) The *Chinese mitten crab* (*Eriocheir sinensis*) showing the body structure and components of a crab. (b) Muscles showing the motion mechanism of the crab leg. (c) Crab-limb inspired novel joint mechanism for legged robots. The rotational joint bends when the flexible thin-wall spring steel sheet (FSSS) pushes. The rotational joint stretches when the FSSS pulls.
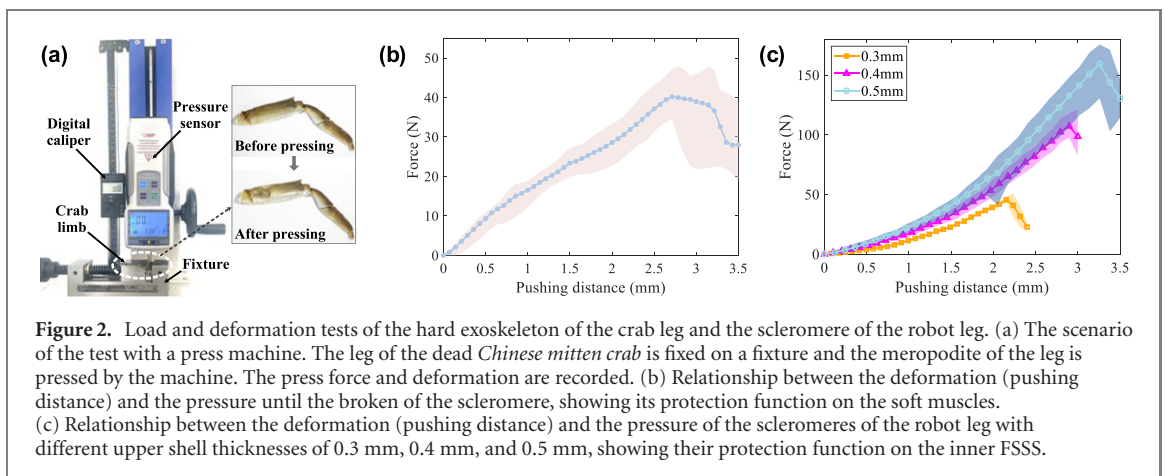

Figure 2. Load and deformation tests of the hard exoskeleton of the crab leg and the scleromere of the robot leg. (a) The scenario of the test with a press machine. The leg of the dead *Chinese mitten crab* is fixed on a fixture and the meropodite of the leg is pressed by the machine. The press force and deformation are recorded. (b) Relationship between the deformation (pushing distance) and the pressure until the broken of the scleromere, showing its protection function on the soft muscles. (c) Relationship between the deformation (pushing distance) and the pressure of the scleromeres of the robot leg with different upper shell thicknesses of 0.3 mm, 0.4 mm, and 0.5 mm, showing their protection function on the inner FSSS.

neighboring legs [44]. The statistical results indicate that the M−M and zigzag models dominate the stepping patterns of the crabs. The motion sequences of the legs during locomotion are shown in figure 3(d). Most crabs use the 4321 and 4231 motion sequences which correspond to the M−M and zigzag models in (c).

3. Crab-inspired robot leg design

Inspired by the structure and motion principle of the crab limb, the novel rigid-flexible coupling compliant leg was designed. Modeling and simulations were also performed to verify the feasibility of the proposed leg design method.

3.1. Compliant leg design
The robot legs should have good compliance and adaptability to walk on different terrains. By studying the structure and motion principle of the crab limb, we designed an under-actuated compliant robot leg consisting of several scleromeres and a thin wall steel sheet. In addition, the kinematics of the leg bending movement was modeled, and the dynamics was analyzed through rigid-flexible coupling simulations.

As the crab-limb-inspired compliant leg illustrated in figure 4(a), the basic principle of the under-

actuated leg is the coupling movement of rigid part and flexible part. The rigid part consists of six scleromeres S1 to S6, like the six parts of the walking leg of crabs in figure 1(a). However, the lengths of the scleromeres S2 to S6 are set as the same to simplify the design and analysis. The scleromeres connected one by one with revolute joints form the outer shell of the robot leg. The FSSS serves as the flexible part of the robot leg, mimicking the muscle inside the hard exoskeleton of crab legs to drive its motion. The FSSS has a trapezoid shape with the base lengths of w and W, the height of L, and the thickness of t. The rear end of the FSSS is connected to the shaft of a linear actuator by a motor connector. The actuator is housed in S1. The front end of the FSSS passes through the narrow slots on S2, S3, S4, and S5 and is fixed at S6. The left-hand and right-hand torsion springs are set at the joints with their two legs installed on the adjacent scleromeres.

The FSSS has the rigidity of force transmission under a pushing force along its L direction. It also possesses flexibility during bending under the squeezing force. The rigidity of the FSSS can realize the bidirectional transferability of an object mounted on it. The FSSS will bend with large deformation when one end is fixed while the other end is pushed. The FSSS straightens again from its bending shape when the moving end is pulled backward. Hence, the joints of
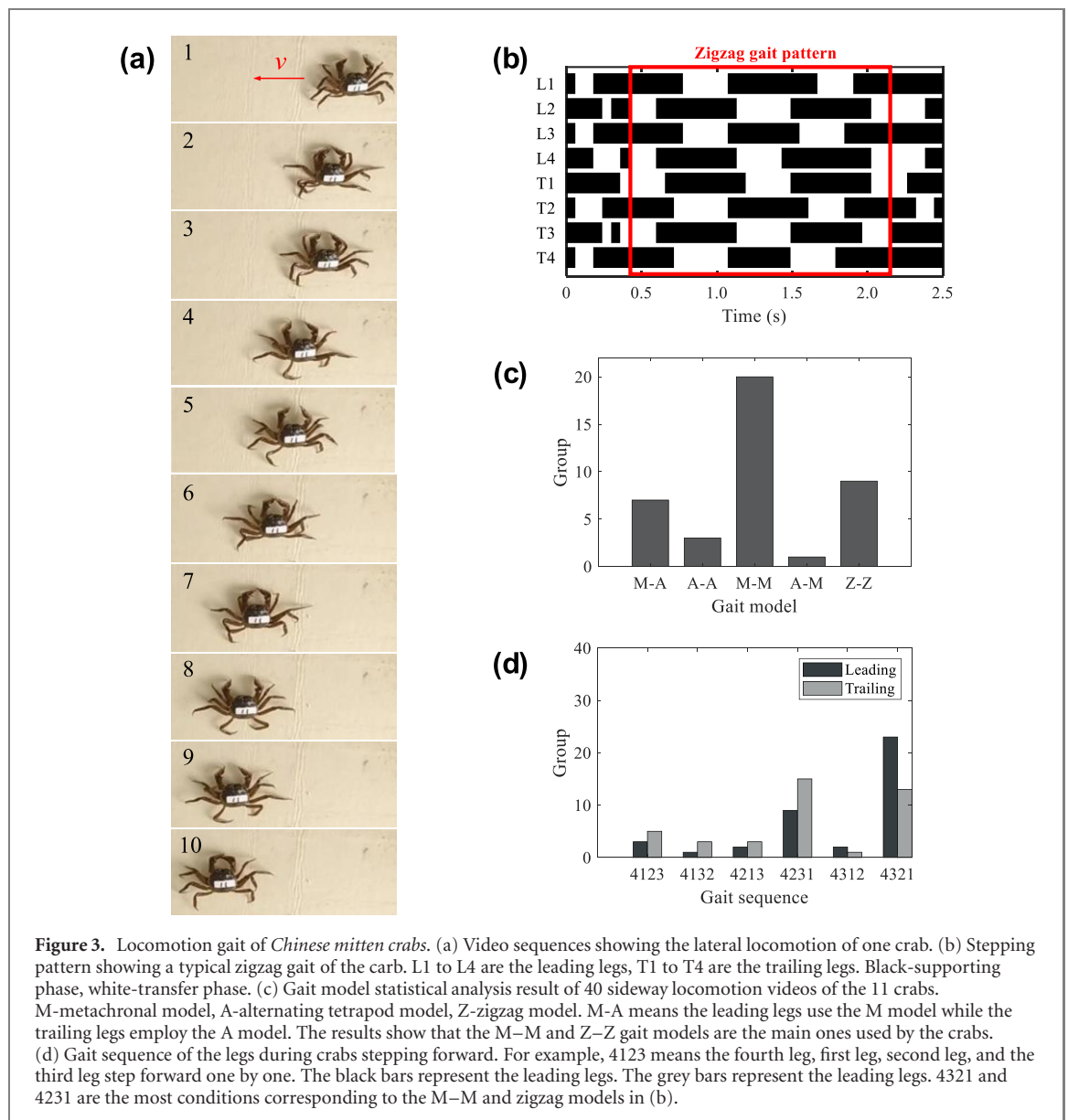
Figure 3. Locomotion gait of *Chinese mitten crabs*. (a) Video sequences showing the lateral locomotion of one crab. (b) Stepping pattern showing a typical zigzag gait of the carb. L1 to L4 are the leading legs, T1 to T4 are the trailing legs. Black-supporting phase, white-transfer phase. (c) Gait model statistical analysis result of 40 sideway locomotion videos of the 11 crabs. M-metachronal model, A-alternating tetrapod model, Z-zigzag model. M-A means the leading legs use the M model while the trailing legs employ the A model. The results show that the M−M and Z−Z gait models are the main ones used by the crabs. (d) Gait sequence of the legs during crabs stepping forward. For example, 4123 means the fourth leg, first leg, second leg, and the third leg step forward one by one. The black bars represent the leading legs. The grey bars represent the leading legs. 4321 and 4231 are the most conditions corresponding to the M−M and zigzag models in (b).
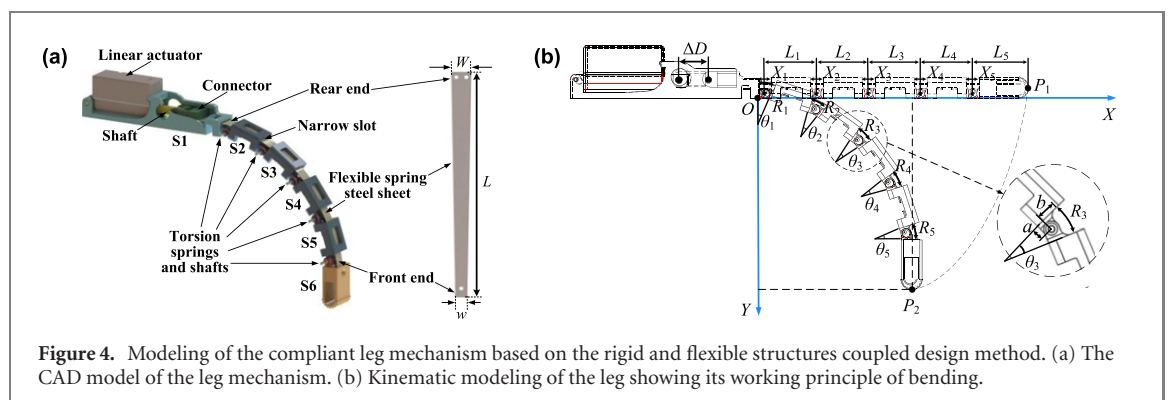
Figure 4. Modeling of the compliant leg mechanism based on the rigid and flexible structures coupled design method. (a) The CAD model of the leg mechanism. (b) Kinematic modeling of the leg showing its working principle of bending.

the scleromeres can rotate for leg bending and stretching when the FSSS is pushed and pulled, respectively. This rigid shell-FSSS coupling design strategy has the merit that the rigid shell can effectively restrict the local buckling of the FSSS and provide contact force for the FSSS, improving its pushing force during the leg bending. This merit enables the leg to bend and

stretch when actuated by just the single motor, realizing a very compact structure of the robot leg like the real crab leg.

Except for the rigid structure and flexible actuation coupling design method, in our robot leg design, the torsion springs are set at the joints of the legs to simulate the joint membrane of the crab limbs. The

torsion springs have two main functions. Firstly, they provide the robot leg with an initial bending angle to avoid the directional uncertainty in the initial bending of the FSSS. Secondly, the torsion springs make the robot leg adaptive to irregular terrain during walking.

3.2. Leg kinematic modeling

Based on the leg design, the leg motion's kinematics modeling was conducted to further explain its working principle. The FSSS slides in the scleromeres S2 to S5 under the thrust at its rear end. As a result, the translational motion achieves the rotational motions of the five joints. By rigid-flexible coupling contact of the FSSS and the rigid shell, the leg is driven by a single linear actuator, achieving a change from a single linear DOF to five under-actuated rotational DOFs.

Figure 4(b) illustrates the diagram of the single-leg bending. L_1 to L_5 are the lengths of S2 to S6, respectively. X_1 to X_5 are the widths of the gaps between the scleromeres, respectively, when the leg is stretched out. R_1 to R_5 depict the arc lengths of the joints while θ_1 to θ_5 represent the rotational angles of the joints, respectively. ΔD is the push displacement of the linear actuator. The details of joint 3 are illustrated in the zoomed-out image. b is the distance of the rotational joint and the FSSS. a is the distance between the joint and the scleromeres. Assuming that every joint has the same rotational angle, we can obtain the relationship between R_i and ΔD as:

$$R_i = \Delta D/n + X_i, \tag{1}$$

where $i = 1, 2, 3, 4, 5$. $n = 5$ is the number of rotational joints. R_i also can be calculated by θ_i as:

$$R_i = \theta_i[b + a/\tan(\theta_i/2)]. \tag{2}$$

The coordinates of the endpoint of the leg can be calculated as:

$$\begin{cases} x = \sum_{i=1}^{n} L_i \times \cos\left(\sum_{j=1}^{j \leqslant i} \theta_i\right) \\ y = \sum_{i=1}^{n} L_i \times \sin\left(\sum_{j=1}^{j \leqslant i} \theta_i\right) \end{cases}, \tag{3}$$

where $j = 1, 2, 3, 4,$ and 5. The coordinates can be used to plan the trajectory of the leg in robot gait design.

3.3. Leg dynamic simulation and stress analysis

Before the legged robot design, we carried out the rigid-flexible coupling dynamic simulations to the compliant leg with the software of Recurdyn (V9R4) to verify the design approach and optimize the parameters of the leg mechanism. The simulation procedure is shown in figure 5(a). The simulation was separated into three steps. In the first step, the scleromeres and FSSS were assembled, and the joints were rotated at a fixed speed to the torsion springs' initial angle of 120°. Secondly, the springs were added at the joints, and the

rotational drive on each joint was removed. Thirdly, a displacement boundary condition within the stroke of the actuator at a trapezoidal speed was applied on the FSSS.

The parameters in the dynamic simulation were set as close to the real leg prototype as possible. The material of the scleromeres and motor connector was set to nylon. The material of the FSSS was spring steel 65 Mn. The material of the shaft was stainless steel. The length, width, and height of the scleromere were 24 mm, 15 mm, and 9.5 mm, respectively, with a slot height of 0.9 mm for passing the FSSS. The size parameters of the FSSS were $L = 127$ mm, $w = 6$ mm, $W = 10$ mm, and $t = 0.2$ mm. The stiffness coefficient of the torsion springs was 25 N mm rad^{-1}.

The pushing force and contact forces between the scleromeres and the FSSS were obtained from the dynamic simulations during the 20 mm pushing of the FSSS and plotted in figure 5(b). The pushing force increases with the displacement of the actuator linearly, with the maximum of about 38 N. The contact forces of the scleromeres S2 to S5 have similar change trends of the quadric curve, with a maximum of about 45 N at the maximum displacement. The endpoint trajectory of the leg was also obtained, as illustrated in figure 5(c). The trajectory is not the same as the one of the crab legs because there is only one active DOF for the robot leg while a least 6 DOFs for the crab leg [34]. The maximum pushing force is used to select the linear actuator in the robot prototype design. The maximum contact forces can be employed to optimize the scleromeres and FSSS.

The stress analyses on the scleromeres and FSSS were performed based on the dynamic simulations before selecting their parameters in the robot design. To check the reliability of the scleromere made of nylon, its most fragile upper shell was selected for stress analysis. In the strength simulation, the maximum force obtained from the dynamic simulation results in figure 5(b) was applied on the inner surface of the shell, where the rigid shells contacted with the FSSS. The stress distribution of the scleromere is illustrated in figure 5(d) when the thickness of the upper shell was 1.0 mm. The lowest safety factors at shell thicknesses 0.2 mm to 1.0 mm are plotted in figure 5(e). The maximum stresses of the parts are smaller than their material yield strengths. The lowest factor of safety is bigger than 1.0 when the thickness is larger than 0.2 mm. Therefore, the strength of the parts can meet the design requirements of robot legs.

The thickness t is an essential parameter that decides the bending ability and stiffness of the FSSS under different pushing forces. We simulated the post-buckling phenomenon of the FSSS. In the simulation, we set a boundary condition with limited freedom in all directions to one side of the FSSS. The other side of the FSSS was only capable of moving in the axial direction. A displacement load from 0 mm to 15 mm at the average speed of 3 mm s^{-1} was applied
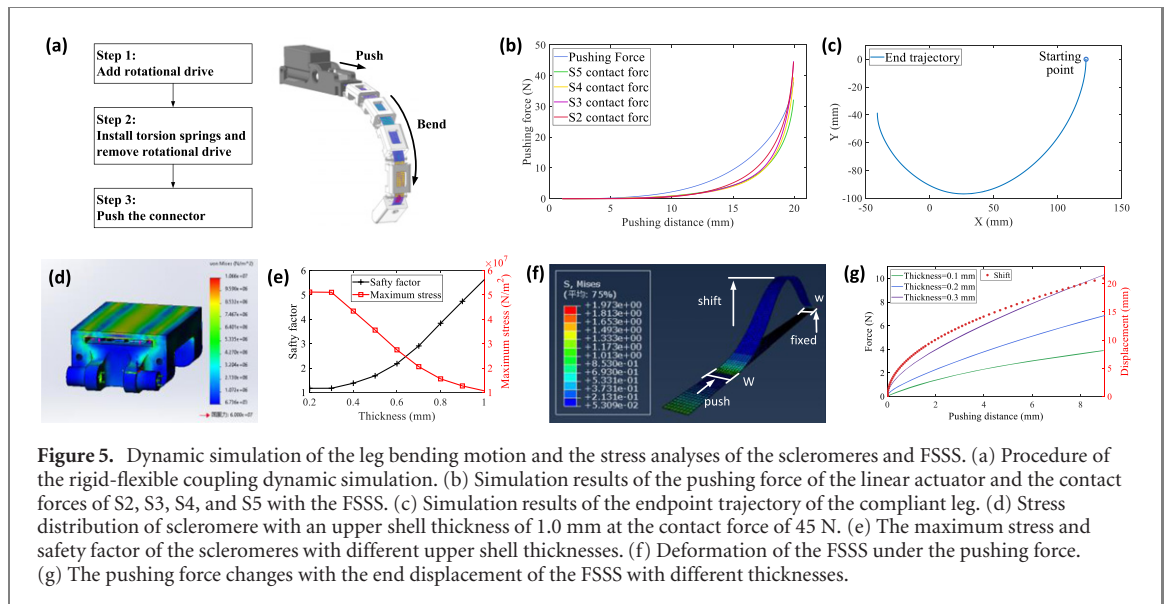
Figure 5. Dynamic simulation of the leg bending motion and the stress analyses of the scleromeres and FSSS. (a) Procedure of the rigid-flexible coupling dynamic simulation. (b) Simulation results of the pushing force of the linear actuator and the contact forces of S2, S3, S4, and S5 with the FSSS. (c) Simulation results of the endpoint trajectory of the compliant leg. (d) Stress distribution of scleromere with an upper shell thickness of 1.0 mm at the contact force of 45 N. (e) The maximum stress and safety factor of the scleromeres with different upper shell thicknesses. (f) Deformation of the FSSS under the pushing force. (g) The pushing force changes with the end displacement of the FSSS with different thicknesses.

on the moving side of the FSSS. From the simulation, we obtained the forces and deformation of the FSSS. Figure 5(f) illustrates the simulation result of the post-buckling analysis when $t = 0.2$ mm. Figure 5(g) shows the push force on the moving end of the FSSS and its shift in the cross-section direction when t is 0.1 mm, 0.2 mm, and 0.3 mm, respectively. The shift of the FSSS is very large while the pushing force is small. Actually, the shift is smaller at a large pushing force, as shown in figure 5(b), because of the restriction of the rigid scleromeres to the FSSS. This demonstrates the unique property of the crab-limb-inspired rigid-flexible coupled leg design method.

4. Crab-inspired legged robot

Based on the crab-limb-inspired novel compliant robotic leg design method, an eight-legged robot was designed to mimic the stepping pattern of its partners. The mechanism, sensing and control system, gait design, and robot prototyping are introduced, respectively.

4.1. Robot design

As illustrated in figure 6(a), the multi-legged robot was designed with the leg design concept. The robot consists of a rectangular body frame, eight walking legs marked from leg 1 to leg 8, a circuit board, and a Li-Po battery. Because of the technical limitation and the main purpose of the leg design method validation with the robot, the legs with the same structure and size are attached symmetrically on the left and right sides of the body frame, which is different from the real crab. The size ratio between the legs and body of the robot is approximate to that of the crab. The body width is reduced a bit to lower the required

thrust of the actuator. The robot is driven by eight linear actuators. The circuit board housed at the bottom of the body frame includes a servo drive unit and an MCU for driving and control of the actuators, a current sensor for current monitoring, an infrared range sensor for detecting the obstacles in front of the robot, an IMU for posture recording, and a WiFi module for commands sending and sensor data transmitting between the robot and a control terminal. The battery is installed on the top of the body frame. The actuators, circuit board, and battery are far from the ground. Hence, the robot could walk in the water when its legs are submerged.

4.2. Gait design

It is significant for the multi-legged robot to have coordinated stepping sequences for different legs to actuate its body moving forward. We designed the locomotion gait of our eight-legged robot based on the crabs' movement patterns and gait models obtained in section 2.

According to the crab locomotion experiments in section 2, the Z–Z model was the main one used by the crabs. Therefore, the Z–Z model, i.e. zigzag gait, was selected for our robot to verify the effectiveness of the design methodology of the single motor actuated compliant robot leg, considering the safety and stability during locomotion. This model was also the selection of the crab-like robot [14]. The robot's stepping pattern is illustrated in figure 6(b). The eight legs are divided into two groups. One group includes leg 1, leg 3, leg 6, and leg 8. The rest of the legs belong to the other group. The steps of the legs in one of the two groups are coincident with each other to make the leg trajectory and software design easier.

Although the leg of the robot has only one actuator, the rigid-flexible coupling design method makes
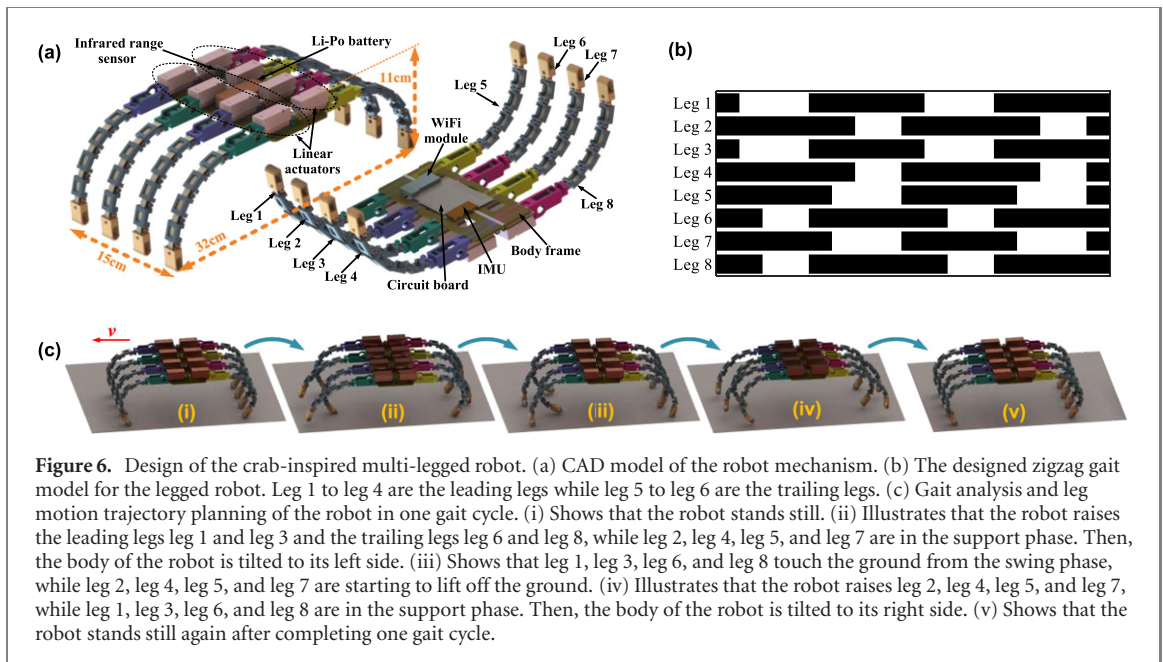
Figure 6. Design of the crab-inspired multi-legged robot. (a) CAD model of the robot mechanism. (b) The designed zigzag gait model for the legged robot. Leg 1 to leg 4 are the leading legs while leg 5 to leg 6 are the trailing legs. (c) Gait analysis and leg motion trajectory planning of the robot in one gait cycle. (i) Shows that the robot stands still. (ii) Illustrates that the robot raises the leading legs leg 1 and leg 3 and the trailing legs leg 6 and leg 8, while leg 2, leg 4, leg 5, and leg 7 are in the support phase. Then, the body of the robot is tilted to its left side. (iii) Shows that leg 1, leg 3, leg 6, and leg 8 touch the ground from the swing phase, while leg 2, leg 4, leg 5, and leg 7 are starting to lift off the ground. (iv) Illustrates that the robot raises leg 2, leg 4, leg 5, and leg 7, while leg 1, leg 3, leg 6, and leg 8 are in the support phase. Then, the body of the robot is tilted to its right side. (v) Shows that the robot stands still again after completing one gait cycle.

the leg possess high flexibility. The dynamic coupling of the legs and body frame enables the legs to lift off the ground and the robot to realize adaptive walking. The locomotion and swing of the legs in one gait cycle are illustrated in figure 6(c). (i) Shows the initial state of the robot that all the legs are in the support phase. As shown in (ii), in the gait cycle, leg 1, leg 3, leg 6, and leg 8 step forward firstly while the rest of the legs are in the support phase. At this moment, the body of the robot is tilted to its left side at an angle because of its gravity. The body is still a tilt to the left side due to the inertia in the movement when leg 1, leg 3, leg 6, and leg 8 are touching the ground. This tilt makes leg 2 and leg 4 have a larger distance to the ground than leg 1 and leg 3, achieving the ground clearance function. In addition, the compliance of the legs enables them to step forward more easily. Leg 5 and leg 7 in the group with leg 2 and leg 4 also can step forward because of the compliance. (iii) depicts that leg 1, leg 3, leg 6, and leg 8 touch the ground from the swing phase, while leg 2, leg 4, leg 5, and leg 7 are starting to lift off the ground. Similarly, the body of the robot is tilted to its right side, as shown in (iv), when the robot raises leg 2, leg 4, leg 5, and leg 7 while leg 1, leg 3, leg 6, and leg 8 are in the support phase. The body tilt makes leg 1 and leg 3 step forward more easily in their next raise. (v) Shows that the robot stands still again after completing one gait cycle. By repeating the above gait cycle, the robot can realize adaptive walking.

The rigid-flexible coupling design methodology and gait design strategy enable the robot to complete adaptive locomotion with only one actuator for each leg. Thus, our robot leg is different from the crab-like robots which employ several motors for each leg [11–14]. In addition, the designed legged robot has the advantages of compact structure and lightweight and is easy to control.

4.3. Fabrication

Based on the design and simulation results, we fabricated a robot prototype for experimental studies. Considering the needed pushing distance of 20 mm and maximum pushing force 38 N of the FSSS during leg bending shown in figure 5(b), the small-sized linear actuator PQ12-R was chosen to drive the robot legs. The linear motor could provide up to 45 N end thrust, with the stroke of 20 mm and the maximum speed of 15 mm s^{-1}. The motor controller PCA9685, a 16-channel 12 bit PWM/servo driver, was chosen to drive the eight linear actuators. The MCU STM32F103RCT6 was chosen as the processor, receiving commands from the PC through WiFi and sending control signals to PCA9685 through the IIC interface. The onboard PWM controller could drive all eight channels simultaneously with no additional STM32 processing overhead. The current sensor MAX471 and the infrared sensor VL53L1X with a range of 0 cm–130 cm were selected for the robot. The whole system was powered by a Li-Po battery (500 mAh, 11.1 V). The body frame and scleromeres were 3D printed of the nylon material with a bending strength of 46.3 MPa and density of 1.28 g cm^{-1}. There were holes designed on the upper and lower surface of the scleromeres for the convenience of 3D printing. The total weight of the legged robot is 437 g.

A gait table calculated from the stepping pattern in figure 6(b) is saved in the MCU. The software running on the PC sends control commands to the robot through WiFi during the robot control. After receiving the control instruction, the MCU then extracts

data stored and refresh the control register of the PCA9685 with a designed frequency. Then, the legs bend and stretch to realize the walking of the robot.

5. Experiments

In order to test the performance of the robot prototype and confirm the rigid-flexible coupled compliant multi-legged robot design methodology, we conducted various experiments, including the leg test and robot locomotion tests.

5.1. Trajectory, compliance, and protection function

The performance of the compliant leg decides the function of the robot. Firstly, the bending experiment of one robot leg was carried out to obtain the leg trajectory and verify the leg simulation results. In this test, the leg was fixed on the desk. The linear actuator moved from 0 mm to 20 mm at a constant speed. This process was recorded by a camera (30 fps and 1920 × 1080 pixels). The video was analyzed by the software Tracker to calculate the rotational angle of each joint and the position of the endpoint. The leg's bending sequences in the simulation and experiment are shown in figures 7(a) and (b), respectively. They have a similar bending trend. To use the simulation results to design the multi-legged robot gait, we have to verify the endpoint trajectory of the robot leg obtained in the simulation. The endpoint trajectories of the leg in experiment and simulation are plotted in figure 7(c). The experiment results are slightly inconsistent with the simulation results. The difference is caused by the complex friction among the parts and the imperfect assembly of the leg prototype. The starting points do not coincide because the leg prototype has an initial bending angle under the torque of the torsion springs. This result suggests that the mechanical design of the robot leg using one linear actuator with the help of the FSSS for driving the multiple rotational joints is feasible.

The compliance of the robot legs was also tested by using the press machine acting on the body frame of the robot when it stood still. The test scenario is illustrated in figure 7(d). The vertical displacement and pressing force are shown in figure 7(e). The tests were non-destructive. The results display a 45 mm deformation at the force of 6.36 N, demonstrating the high compliance of the flexible-rigid structures combined robotic legs. The compliant legs could improve the safety and adaptability during the locomotion of the robot.

The protection function of the scleromeres was also tested. Scleromeres printed of nylon material were used in the destructive testing like the hard exoskeleton pressing test in figure 2(a). The upper shell thicknesses 0.3 mm, 0.4 mm, and 0.5 mm of the scleromeres were selected because of the defect of the 3D printing technology for thin wall printing. The results are shown in figure 2(c). The maximum reaction force of the 0.3 mm thicknesses shell is close to the crab-limbs with the average shell thickness of 0.23 mm. The other two kinds of scleromeres can withstand larger pressure far beyond the contact forces obtained in dynamic simulations. The scleromeres pressing testing results indicate the excellent protection performance of the scleromeres on the inner FSSS.
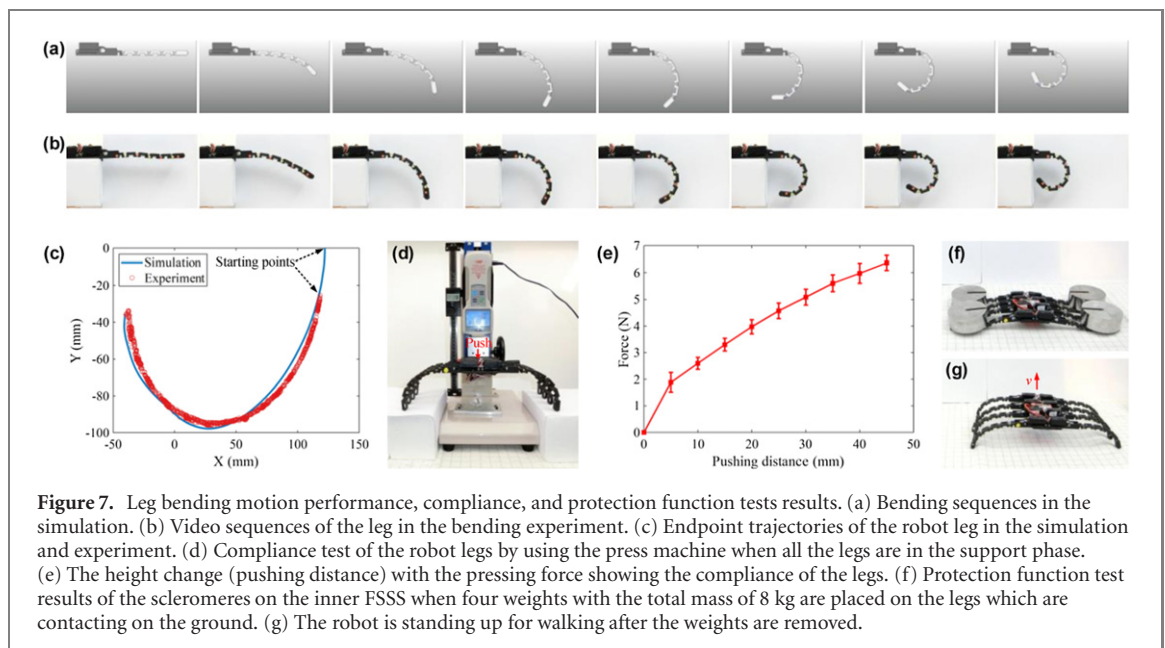
We also performed the protection function tests of the scleromeres. Firstly, the robot stretched its legs until all of them contacted the ground. Then, four weights with a total mass of 8 kg, about 20 times the mass of the robot, were placed on the leading legs and the trailing legs, as illustrated in figure 7(f). Thirdly, the robot stood up after all the weights were removed, as shown in figure 7(g). Finally, the robot walked again with the legs intact. The complete process can be seen in the attached video S1 (https://stacks.iop.org/BB/17/025001/mmedia) of the paper. The results demonstrated that the robot could withstand very large pressure with the protection of the scleromeres in some applications like search and rescue. The results also proved the biological superiority of the crab's legs structure from the engineering point of view.

5.2. Adaptive locomotion on different terrains

In this section, numerous walking experiments of the multi-legged robot were carried out to test its walking adaptability on different terrains. We recorded the videos of the robot walking by the camera. The position and velocity of the robot were obtained by tracking a marker pasted on the body frame with Tracker. The power of the robot was calculated with the current measured through the current sensor and the 6 V voltage of the actuators.

Firstly, the robot walking using the designed zigzag gait was tested. In this experiment, the robot walked with designed control paraments from the gait model in figure 6(b) to imitate the walking of crabs. Figure 8(a) illustrates the video sequences of the robot walking with the zigzag gait where leg 1, leg 3, leg 6, and leg 8 form group 1, while leg 2, leg 4, leg 5, and leg 7 form group 2. The locomotion displacements in the horizontal and vertical directions are plotted in figure 8(c). As the robot walks forward, the horizontal displacement shows a stepped rise, and the vertical one shows periodic fluctuations, which are in line with the expectation.

The body roll angle change and power consumption of the robot during walking are illustrated in figure 8(d). The angle and power have periodic fluctuations consistent with the swing of the legs and the push and pull of the linear actuators. As expected, the alternate rising and falling of the left and right sides of the body enable the legs to have the ground clearance capability and the robot to walk adaptively. The

Figure 7. Leg bending motion performance, compliance, and protection function tests results. (a) Bending sequences in the simulation. (b) Video sequences of the leg in the bending experiment. (c) Endpoint trajectories of the robot leg in the simulation and experiment. (d) Compliance test of the robot legs by using the press machine when all the legs are in the support phase. (e) The height change (pushing distance) with the pressing force showing the compliance of the legs. (f) Protection function test results of the scleromeres on the inner FSSS when four weights with the total mass of 8 kg are placed on the legs which are contacting on the ground. (g) The robot is standing up for walking after the weights are removed.

result is consistent with the gait design and analysis of the robot and verifies the feasibility of one motor actuated flexible-rigid coupling compliant leg design methodology.

Secondly, the influence of the control parameters on the walking performance of the robot was studied. The gait frequency increased from 0.57 Hz to 1.14 Hz. We performed the test at different frequencies five times when the robot walked with the zigzag gait. The speed and the power of the robot are demonstrated in figure 8(e). The velocity and power consumption of the robot all have no noticeable change when the frequency is lower than 0.74 Hz or higher than 0.86 Hz. However, the velocity increases significantly while the power has a slight rise from 0.74 Hz to 0.86 Hz.
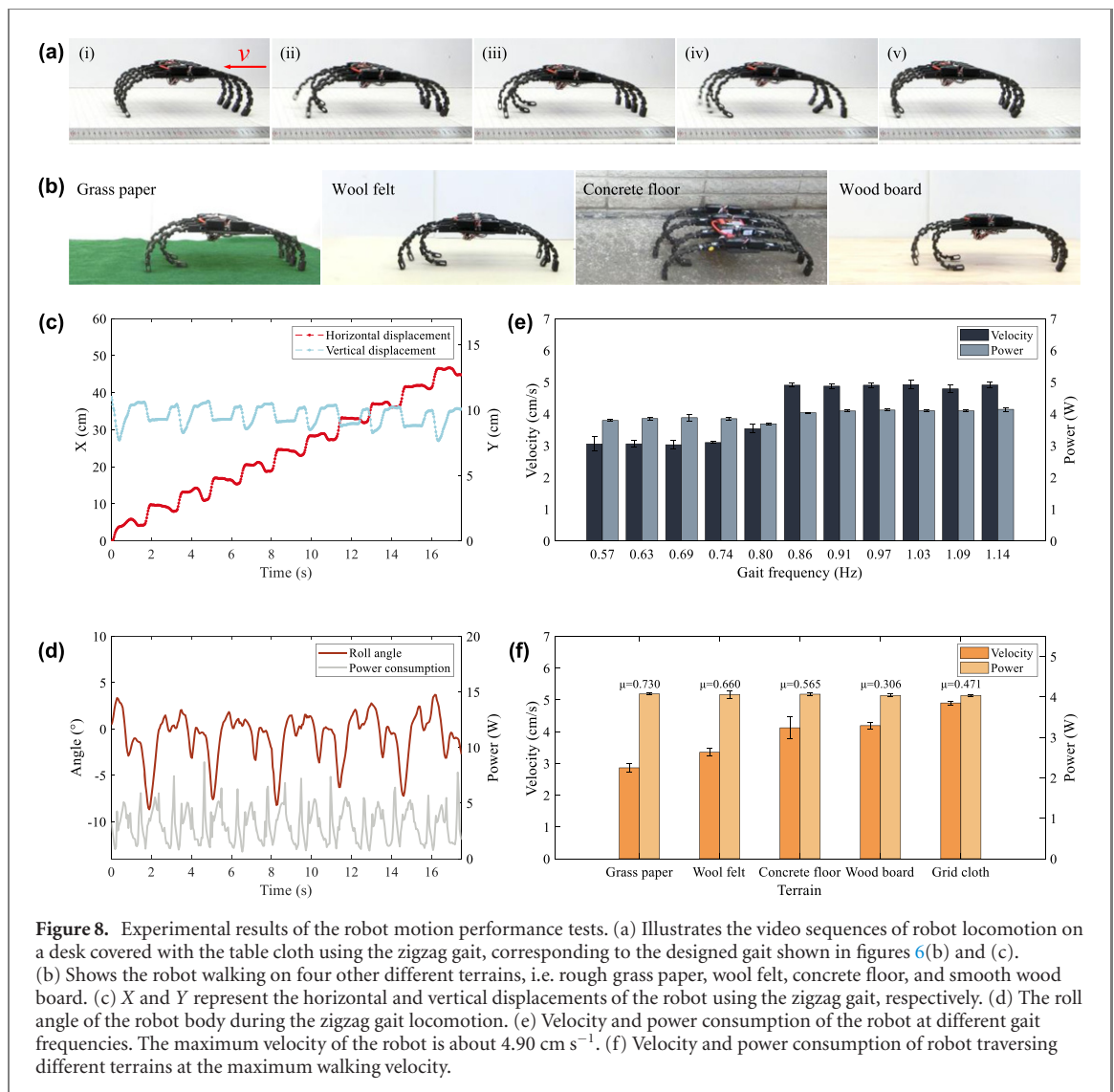
Finally, the effect of different terrains with different coefficients of friction on the walking performance of the robot was investigated. Before the experiments, the coefficients of friction between the robot leg tip and the terrains, i.e. grid cloth, rough grass paper, wool felt, concrete floor, and smooth wood board were tested with a force gauge and a weight. Then, the robot walked on the five different terrains with the zigzag gait and gait frequency of 0.86 Hz. A video of the robot walking on the terrains is available as the attached movie S2. Figure 8(a) shows the snapshots of the robot walking on the grid cloth, while figure 8(b) illustrates the snapshots of it moving on other terrains. The tests on different terrains were conducted five times, respectively. The average walking velocity, power consumption, and the coefficients of friction between the leg tip of the robot and the terrains in the tests are plotted in figure 8(f). The power consumption in each test is almost the same as about 4 W. The Li-Po battery can provide about 83 min of power for the robot walking (considering the average current of the actuators as 650 mA at 6 V voltage). The robot walks fastest on the grid cloth, about

4.90 cm s^{-1}. The results imply that the smaller the coefficient of friction, the larger the robot's walking speed. The result on the wood board is an exception caused by the too smooth and slippery surface of the board.

These experiments verify that the multi-legged robot can walk steadily forward on different terrains with the crab-inspired gaits designed in the previous section. The results also demonstrate that the walking velocity of the robot can be easily controlled by changing the gait frequency.

5.3. Low channel traversing like a crab
In this paper, the bionic behavior of the robot was also an essential research purpose of the robot design with compliant legs. Here our goal was to imitate the avoidance behavior of the crab, hiding in rock crevices or low burrows [45]. The experiment was performed to test the channel crossing ability of the robot. A video of the robot traversing the channel can be seen in the attached movie S3. The snapshots of the robot crossing a 10 cm high channel are illustrated in figure 9(a). In the test, the robot was placed in front of the channel firstly. Then, the robot walked and approached the channel with a body height of about 11 cm. The infrared range sensor installed on the robot with a tilt detected the distance from the obstacle. When the sensor detected a sudden change of the distance, the robot adjusted the pushing distance of the actuators in the gait automatically until it could walk in the channel. Thirdly, the robot walked through the channel with a lowered body height of about 9.76 cm. Finally, the robot adjusted its body height and gait to the normal conditions when it could not detect the obstacle above its head. The body height change of the robot is shown in figure (b). Its height decreases before it crosses the channel and increases to the normal one again after it walks out of the channel.

Figure 8. Experimental results of the robot motion performance tests. (a) Illustrates the video sequences of robot locomotion on a desk covered with the table cloth using the zigzag gait, corresponding to the designed gait shown in figures 6(b) and (c). (b) Shows the robot walking on four other different terrains, i.e. rough grass paper, wool felt, concrete floor, and smooth wood board. (c) *X* and *Y* represent the horizontal and vertical displacements of the robot using the zigzag gait, respectively. (d) The roll angle of the robot body during the zigzag gait locomotion. (e) Velocity and power consumption of the robot at different gait frequencies. The maximum velocity of the robot is about 4.90 cm s^{-1}. (f) Velocity and power consumption of robot traversing different terrains at the maximum walking velocity.
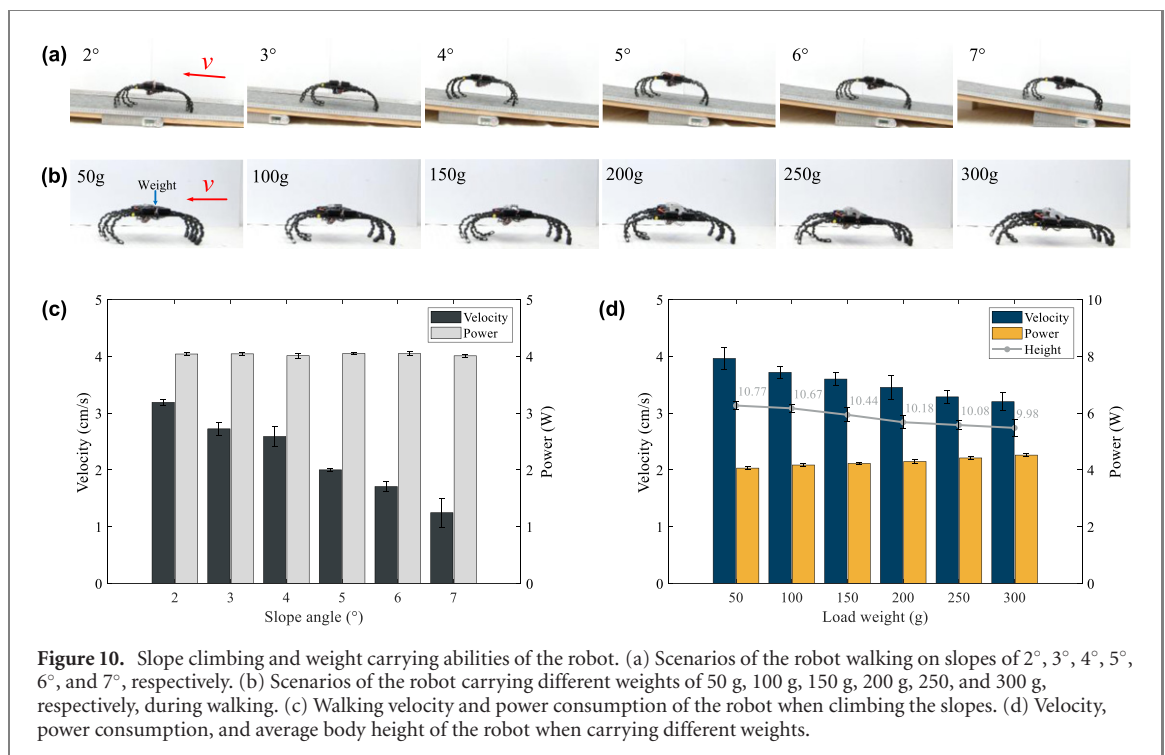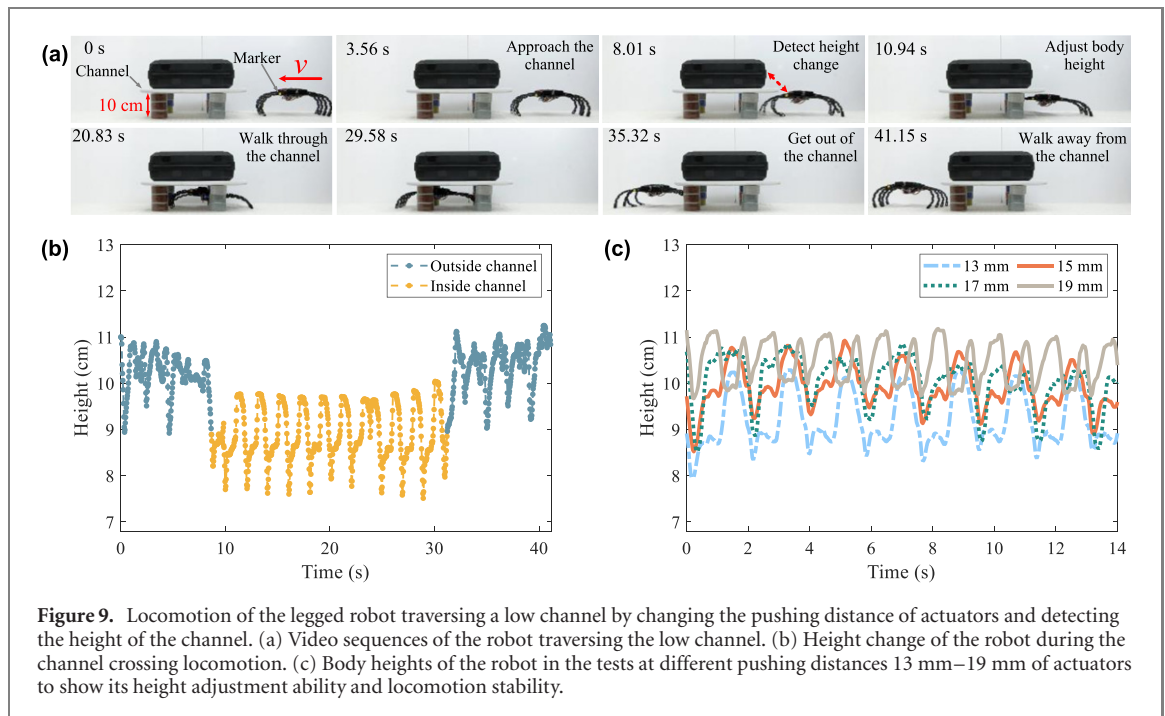
To help design the channel traversing experiment, we also tested the body height adjustment ability of the robot. Figure 9(c) depicts the body height variation with different gait patterns, i.e. different ranges of the pushing distance of the actuator within the maximum 20 mm stroke. The results show that the robot's body height is lower when the actuators' pushing distance is shorter. However, the height variation amplitude has an opposite change trend. This conclusion is helpful for the height adjustment and stability improvement of the multi-legged robot. Thus, the channel crossing experiment proves that the robot can adjust the body height to adapt to the environment change like a real crab. This ability is important for the robot and crab because the height adjustment, i.e. stance changing, is also essential for them to keep a proper distance between their body and the uneven, unpredictable surface to avoid body injury [43]. Furthermore, low body height also means a large support area which improves locomotion stability.

5.4. Slope climbing and weight carrying

Based on the walking experiments of the robot on different terrains at different control parameters,

we also carried out two other experiments to test its slope climbing and weight carrying capabilities. Figure 10(a) shows the snapshots of the robot climbing different slopes from 2° to 7°. Figure 10(c) represents the walking speed and power of the robot when climbing the slopes. It is evident that the speed drops quickly with the increase of the slope angle because the stepping of the compliant leg is harder on the slope than that on the ground. However, the energy consumption seems to have no significant change at different slopes for the same control parameters of the robot. A video of the robot walking on the slopes is available as the attached movie S4.

Weight carrying ability is also an essential part of robot design. The robot carried six kinds of weights from 50 g to 300 g, respectively, during the walking tests, as seen in the attached movie S5. The video sequences of the robot during the loading experiment are illustrated in figure 10(b). The average walking velocity, power, and body height recorded in the tests are plotted in figure 10(d). The results indicate that the velocity and body height all decline with the increase of the load weight while the power has

Figure 9. Locomotion of the legged robot traversing a low channel by changing the pushing distance of actuators and detecting the height of the channel. (a) Video sequences of the robot traversing the low channel. (b) Height change of the robot during the channel crossing locomotion. (c) Body heights of the robot in the tests at different pushing distances 13 mm−19 mm of actuators to show its height adjustment ability and locomotion stability.

Figure 10. Slope climbing and weight carrying abilities of the robot. (a) Scenarios of the robot walking on slopes of 2°, 3°, 4°, 5°, 6°, and 7°, respectively. (b) Scenarios of the robot carrying different weights of 50 g, 100 g, 150 g, 200 g, 250, and 300 g, respectively, during walking. (c) Walking velocity and power consumption of the robot when climbing the slopes. (d) Velocity, power consumption, and average body height of the robot when carrying different weights.

an increasing change trend. These results are consistent with expectations. The results in this subsection reveal that the multi-legged robot can climb a slope and carry weights up to 300 g, about 69% of its weight. These abilities are helpful for the robot to add more sensors and actuators in the applications such as environmental monitoring.

6. Conclusions and future work

This work presents the design and implementation of a multi-legged robot borrowing the biological structure and stepping pattern of the *Chinese mitten crab*. The rigid exoskeleton structure and flexible internal actuation mechanism of the crab limb were analyzed, and a large number of the robot's walking videos were recorded. Their gaits were classified by statistical analysis of the video sequences. Based on the crab research, we designed the multi-legged robot consisting of eight compliant legs.

Firstly, the rigid-flexible compliant leg design method was proposed and verified by the kinematic modeling, rigid-flexible coupled dynamic simulation, and stress analysis. Then, the robot's gait was

designed, imitating the gaits of the crabs and considering the characteristics of the compliant legs and their coupling effect with the rigid body frame during walking. Thirdly, the mechanical parts of the robot were manufactured via 3D printing technology, and the sensing and control system was implemented.

Finally, many kinds of experiments were carried out to validate the design approach and performance of the robot. The single-leg bending experiments, leg compliance tests, and robot static loading tests verified the design methodology of the compliant leg. The velocity, energy consumption, and repeatability of the robot locomotion with the designed zigzag gait model were evaluated by many experiments. The maximum speed was about 4.90 cm s^{-1} with a power of 4.07 W. The terrain adaptability was tested when the robot walked on five different terrains, i.e. grid cloth, rough grass paper, wool felt, concrete floor, and smooth wood board. The results indicated that the robot could walk on the different terrains adaptively and had the highest walking speed on the grid cloth with the proper coefficient of friction, not too big or too small. Other experiments, including low channel traversing, slope climbing, and weight carrying, were also performed. The results demonstrated that the robot could cross the channel like a crab by lowering its body height through adjusting the control parameters. The robot had the ability to walk on a slope with an angle of 7° smoothly and adaptively. The robot was able to carry an object of 300 g, about 69% of its weight, which is a large capacity for adding cameras or other sensors to the robot. The experimental results of the robot walking at different speeds, with different body heights, on different terrains, on different slops, and carrying different loads can be seen in the attached videos of this paper. The results prove that the single-motor-actuated compliant legs and their dynamic coupling with the rigid body frame can enable them to have the ground clearance ability and realize the adaptive walking of the robot. The robot could also cross the shallow water when the lower half of its legs is submerged because the electronic components, including actuators, circuit board, and battery, are at the top of the body frame and far from the water.

Although the novel flexible-rigid structures combined design strategy makes the robot compact, light, and easy to control, some efforts could also be made, such as structure optimization, waterproof enclosure design, leg bending angle closed-loop control, and other kinds of gaits design (like turning gait), to improve the locomotion efficiency and obstacle overcoming ability. Furthermore, additional sensors like the mini camera, sound sensor, and carbon dioxide sensor will be integrated into an advanced circuit board with a more powerful processing capability for the environmental monitoring application.

Data availability statement

All data that support the findings of this study are included within the article (and any supplementary files).

ORCID iDs

Jun Zhang ⓘ https://orcid.org/0000-0002-3074-2465
Qi Liu ⓘ https://orcid.org/0000-0001-5444-8810
Jingsong Zhou ⓘ https://orcid.org/0000-0002-1596-9645
Aiguo Song ⓘ https://orcid.org/0000-0002-1982-6780

References

[1] Kajita S and Espiau B 2008 Legged robots *Springer Handbook of Robotics* (Berlin: Springer) pp 361–89
[2] Luk B L, Galt S and Galt S 2001 Using genetic algorithms to establish efficient walking gaits for an eight-legged robot *Int. J. Syst. Sci.* **32** 703–13
[3] Biswal P and Mohanty P K 2020 Development of quadruped walking robots: a review *Ain Shams Eng. J.* **12** 2017–31
[4] He J and Gao F 2020 Mechanism, actuation, perception, and control of highly dynamic multilegged robots: a review *Chin. J. Mech. Eng.* **33** 79
[5] Semini C and Wieber P-B 2020 *Encycl. Robot.* (Berlin: Springer) pp 1–8
[6] Poulakakis I *et al* 2017 Legged robots with bioinspired morphology *Bioinspired Legged Locomotion: Models, Concepts, Control and Applications* (Oxford: Butterworth-Heinemann) pp 457–561
[7] Raibert M, Blankespoor K, Nelson G and Playter R 2008 BigDog, the rough-terrain quadruped robot *World Congress* vol 41 pp 10822–5
[8] Park H-W, Wensing P M and Kim S 2021 Jumping over obstacles with MIT Cheetah 2 *Robot. Autonom. Syst.* **136** 103703
[9] Moore E Z, Campbell D, Grimminger F and Buehler M 2002 Reliable stair climbing in the simple hexapod 'RHex' *IEEE Int. Conf. Robotics and Automation (ICRA)* vol 3 pp 2222–7
[10] Chou Y-C, Yu W-S, Huang K-J and Lin P-C 2012 Bio-inspired step-climbing in a hexapod robot *Bioinspiration Biomimetics* **7** 036008
[11] Safak K K and Adams G G 2002 Modeling and simulation of an artificial muscle and its application to biomimetic robot posture control *Robot. Autonom. Syst.* **41** 225–43
[12] Anon 2004 News—spider-bots are go! *IEE Rev.* **50** 10
[13] Yoo S-y, Shim H, Jun B-H, Park J-Y and Lee P-M 2016 Design of walking and swimming algorithms for a multi-legged underwater robot crabster CR200 *Mar. Technol. Soc. J.* **50** 74–87

[14] Chen X, Wang L-q, Ye X-f, Wang G and Wang H-l 2013 Prototype development and gait planning of biologically inspired multi-legged crablike robot *Mechatronics* **23** 429–44

[15] Graf N M, Behr A M and Daltorio K A 2021 Dactyls and inward gripping stance for amphibious crab-like robots on sand *Bioinspiration Biomimetics* **16** 026021

[16] Fukuoka Y, Kimura H, Hada Y and Takase K 2003 Adaptive dynamic walking of a quadruped robot 'Tekken' on irregular terrain using a neural system model *IEEE Int. Conf. Robotics and Automation (ICRA)* vol 2 pp 2037–42

[17] Buchli J and Ijspeert A J 2008 Self-organized adaptive legged locomotion in a compliant quadruped robot *Autonom. Robot.* **25** 331–47

[18] Lee H, Shen Y, Yu C H, Singh G and Ng A Y 2006 Quadruped robot obstacle negotiation via reinforcement learning *IEEE Int. Conf. Robotics and Automation (ICRA)* pp 3003–10

[19] Hwangbo J, Lee J, Dosovitskiy A, Bellicoso D, Lee J, Tsounis V, Koltun V and Hutter M 2019 Learning agile and dynamic motor skills for legged robots *Sci. Robot.* **4** 26

[20] Zhang C, An H, Wu C, Lang L, Wei Q and Ma H 2020 Contact force estimation method of legged-robot and its application in impedance control *IEEE Access* **8** 161175–87

[21] Goldschmidt D, Wörgötter F and Manoonpong P 2014 Biologically-inspired adaptive obstacle negotiation behavior of hexapod robots *Front. Neurorobot.* **8** 1–16

[22] Vandesompele A, Urbain G, Wyffels F and Dambre J 2019 Populations of spiking neurons for reservoir computing: closed loop control of a compliant quadruped *Cognit. Syst. Res.* **58** 317–23

[23] Liu X, Rossi A and Poulakakis I 2018 A switchable parallel elastic actuator and its application to leg design for running robots *IEEE/ASME Trans. Mechatron.* **23** 2681–92

[24] Spröwitz A, Tuleu A, Vespignani M, Ajallooeian M, Badri E and Ijspeert A J 2013 Towards dynamic trot gait locomotion: design, control, and experiments with Cheetah-cub, a compliant quadruped robot *Int. J. Rob. Res.* **32** 932–50

[25] Hutter M, Gehring C, Hopflinger M A, Blosch M and Siegwart R 2014 Toward combining speed, efficiency, versatility, and robustness in an autonomous quadruped *IEEE Trans. Robot.* **30** 1427–40

[26] Gor M M, Pathak P M, Samantaray A K, Yang J-M and Kwak S W 2015 Control oriented model-based simulation and experimental studies on a compliant legged quadruped robot *Robot. Autonom. Syst.* **72** 217–34

[27] Hoffmann M and Simanek J 2017 The merits of passive compliant joints in legged locomotion: fast learning, superior energy efficiency and versatile sensing in a quadruped robot *J. Bionic Eng.* **14** 1–14

[28] Kanner O Y, Rojas N, Odhner L U and Dollar A M 2017 Adaptive legged robots through exactly constrained and non-redundant design *IEEE Access* **5** 11131–41

[29] Lakatos D, Ploeger K, Loeffl F, Seidel D, Schmidt F, Gumpert T, John F, Bertram T and Albu-Schaffer A 2018 Dynamic locomotion gaits of a compliantly actuated quadruped with SLIP-like articulated legs embodied in the mechanical design *IEEE Robot. Autom. Lett.* **3** 3908–15

[30] Sun J and Zhao J 2019 An adaptive walking robot with reconfigurable mechanisms using shape morphing joints *IEEE Robot. Autom. Lett.* **4** 724–31

[31] Sharbafi M A, Yazdanpanah M J, Ahmadabadi M N and Seyfarth A 2020 Parallel compliance design for increasing robustness and efficiency in legged locomotion-proof of concept *IEEE/ASME Trans. Mechatron.* **24** 1541–52

[32] Mahkam N and Özcan O 2021 Gait and locomotion analysis of a soft-hybrid multi-legged modular miniature robot *Bioinspiration Biomimetics* **16** 066009

[33] Picardi G, Chellapurath M, Iacoponi S, Stefanni S, Laschi C and Calisti M 2020 Bioinspired underwater legged robot for seabed exploration with low environmental disturbance *Sci. Robot.* **5** 1–14

[34] Wang G, Chen X, Yang S, Jia P, Yan X and Xie J 2017 Subsea crab bounding gait of leg-paddle hybrid driven shoal crablike robot *Mechatronics* **48** 1–11

[35] Kim S, Laschi C and Trimmer B 2013 Soft robotics: a bioinspired evolution in robotics *Trends Biotechnol.* **31** 287–94

[36] Shepherd R F, Ilievski F, Choi W, Morin S A, Stokes A A, Mazzeo A D, Chen X, Wang M and Whitesides G M 2011 Multigait soft robot *Proc. Natl Acad. Sci.* **108** 20400–3

[37] Fang T, Zhou Y, Li S, Xu M, Liang H, Li W and Zhang S 2016 Theoretical and experimental study on a compliant flipper-leg during terrestrial locomotion *Bioinspiration Biomimetics* **11** 056005

[38] Kaln M A I, Aygul C, Turkmen A, Kwiczak-Yigitbas J, Baytekin B and Ozcan O 2020 Design, fabrication, and locomotion analysis of an untethered miniature soft quadruped, SQuad *IEEE Robot. Autom. Lett.* **5** 3854–60

[39] Zhou D, Zuo W, Tang X, Deng J and Liu Y 2021 A multi-motion bionic soft hexapod robot driven by self-sensing controlled twisted artificial muscles *Bioinspiration Biomimetics* **16** 045003

[40] Yoshida Y, Yamauchi K, Hiraragi R, Kiyono Y, Omori S and Shibano J-i 2020 Microstructures of crab chela: a biological composite for pinching *J. Mech. Behav. Biomed. Mater.* **112** 104071

[41] Vidal-Gadea A G and Belanger J H 2009 Muscular anatomy of the legs of the forward walking crab, Libinia emarginata (Decapoda, Brachyura, Majoidea) *Arthropod Struct. Dev.* **38** 179–94

[42] Sleinis S and Silvey G E 1980 Locomotion in a forward walking crab *J. Comp. Physiol.* **136** 301–12

[43] Hui C A 1992 Walking of the shore crab Pachygrapsus crassipes in its two natural environments *J. Exp. Biol.* **165** 213–27

[44] Barnes W J P 1975 Leg co-ordination during walking in the crab, Uca pugnax *J. Comp. Physiol.* **96** 237–56

[45] Jennions M D, Backwell P R Y, Murai M and Christy J H 2003 Hiding behaviour in fiddler crabs: how long should prey hide in response to a potential predator? *Anim. Behav.* **66** 251–7